Supporting Information

Molecular magnetism and Solid-Phase Transformations of Dy, Er, Yb tropolonate complexes

Svetlana P. Petrosyants, Konstantin A. Babeshkin, Alina S. Galkina,* Andrey B. Ilyukhin, Nikolay N. Efimov and Igor L. Eremenko.

N.S. Kurnakov Institute of General and Inorganic Chemistry, Russian Academy of Sciences, Leninsky prosp. 31, 119991 Moscow, Russian Federation.

Email: asgalkina@bk.ru

Table S1. Crystal data and structure refinement for **1Ln**, **2Ln**.

Identification code	**1Er**	**2Er**	**2Yb_150K**	**2Yb_296K**
Empirical formula	$C_{21}H_{20}ErO_{8.50}$	$C_{28}H_{21}ErO_8$	$C_{28}H_{21}O_8Yb$	$C_{28}H_{21}O_8Yb$
Formula weight	575.63	652.71	658.49	658.49
Temperature, K	150(2)	150(2)	150(2)	296(2)
Wavelength, Å	0.71073	0.71073	0.71073	0.71073
Crystal system	Monoclinic	Triclinic	Triclinic	Triclinic
Space group	$P2_1/c$	P-1	P-1	P-1
a, Å	21.3411(8)	10.0449(5)	10.0295(4)	10.0839(4)
b, Å	6.4416(2)	11.4689(6)	11.4586(4)	11.5409(5)
c, Å	28.9639(10)	12.1580(6)	12.1143(5)	12.1372(5)
α, °	90	73.4297(15)	73.3230(10)	73.3888(14)
β, °	98.5854(11)	84.9764(16)	84.9470(10)	84.9290(14)
γ, °	90	64.7027(15)	64.8260(10)	64.9723(13)
Volume, $Å^3$	3937.1(2)	1212.79(11)	1206.07(8)	1225.59(9)
Z	8	2	2	2
D (calc), Mg/m^3	1.942	1.787	1.813	1.784
μ, mm^{-1}	4.314	3.512	3.929	3.867
F(000)	2256	642	646	646
Crystal size, mm	0.24 x 0.20 x 0.20	0.28 x 0.24 x 0.10	0.30 x 0.24 x 0.22	0.20 x 0.18 x 0.12
θ range, °	2.220, 26.372	2.295, 27.485	2.604, 33.176	2.285, 34.348
Index ranges	-26<=h<=26 -8<=k<=8 -36<=l<=36	-13<=h<=13 -14<=k<=14 -15<=l<=15	-15<=h<=15 -17<=k<=17 -18<=l<=18	-14<=h<=15 -18<=k<=16 -17<=l<=19
Reflections collected	49336	15999	25152	25749
Independent reflections, Rint	8014, 0.0424	5544, 0.0416	8446, 0.0405	8722, 0.0257
Completeness to θ = 25.242°	99.9 %	99.8 %	99.8 %	99.5 %
Absorption correction	Semi-empirical from equivalents	Semi-empirical from equivalents	Semi-empirical from equivalents	Semi-empirical from equivalents
Max,. min. transmission	0.2657, 0.1785	0.5110, 0.1960	0.7465, 0.3528	0.7468, 0.5135
Refinement method	Full-matrix least-squares on F^2	Full-matrix least-squares on F^2	Full-matrix least-squares on F^2	Full-matrix least-squares on F^2
Data / restraints / parameters	8014 / 6 / 551	5544 / 0 / 334	8446 / 0 / 341	8722 / 0 / 334
Goodness-of-fit	1.135	1.091	1.124	1.028
R1, wR2 [I>2sigma(I)]	0.0264, 0.0597	0.0429, 0.0949	0.0262, 0.0548	0.0222, 0.0465
R1, wR2 (all data)	0.0303, 0.0614	0.0510, 0.0977	0.0290, 0.0557	0.0261, 0.0478
Largest diff. peak and hole, $e.Å^{-3}$	0.912, -0.866	1.484, -2.408	1.913, -1.782	0.625, -0.602

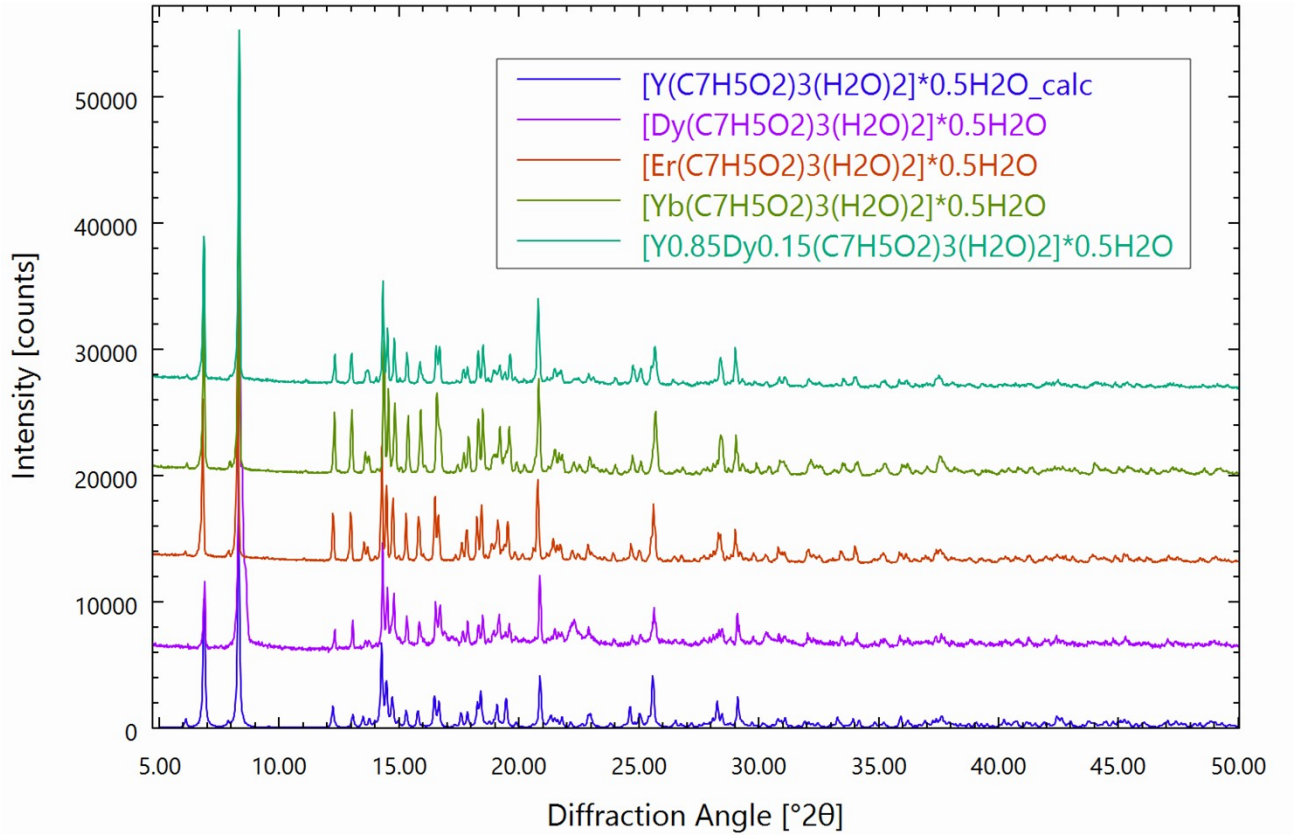
[Y(C7H5O2)3(H2O)2]*0.5H2O_calc
[Dy(C7H5O2)3(H2O)2]*0.5H2O
[Er(C7H5O2)3(H2O)2]*0.5H2O
[Yb(C7H5O2)3(H2O)2]*0.5H2O
[Y0.85Dy0.15(C7H5O2)3(H2O)2]*0.5H2O
Intensity [counts]
Diffraction Angle [°2θ]

(a)

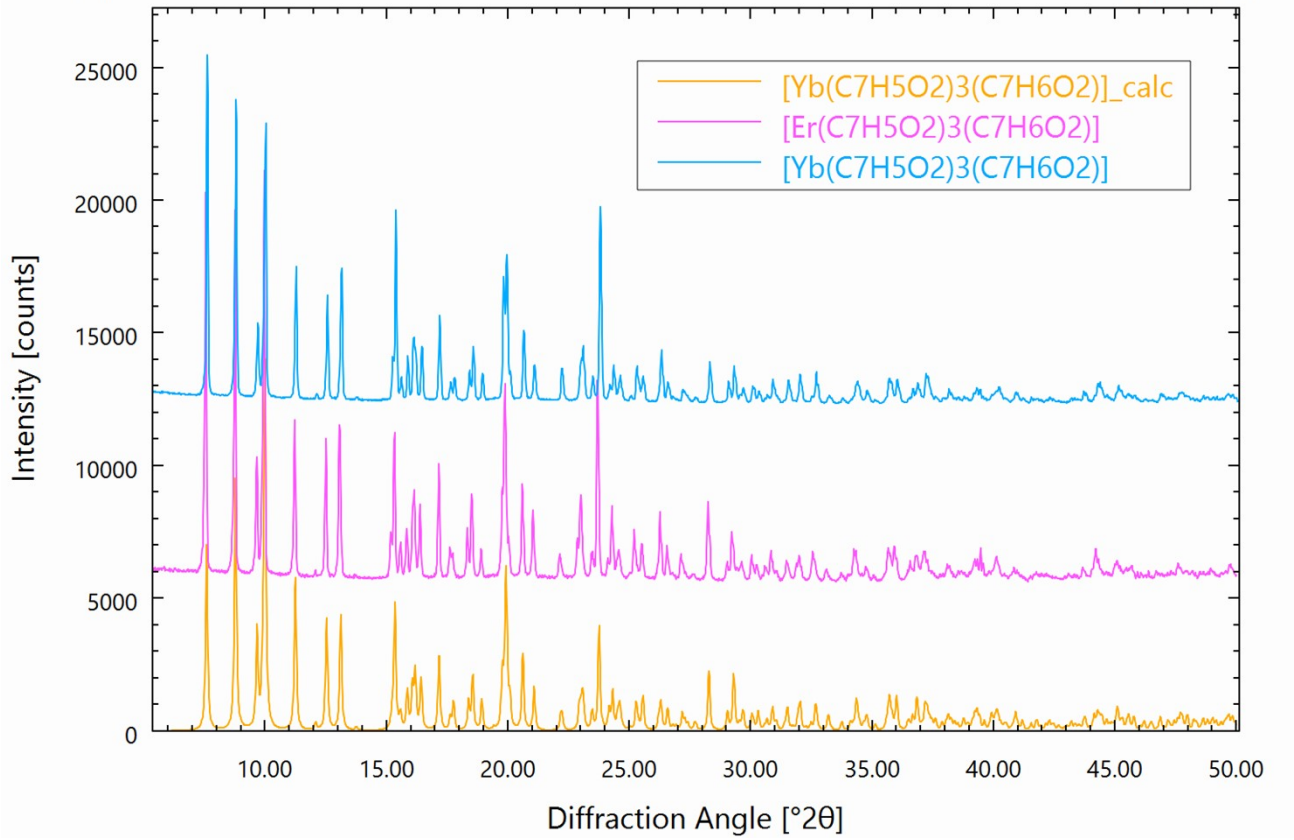
[Yb(C7H5O2)3(C7H6O2)]_calc
[Er(C7H5O2)3(C7H6O2)]
[Yb(C7H5O2)3(C7H6O2)]
Intensity [counts]
Diffraction Angle [°2θ]

(b)

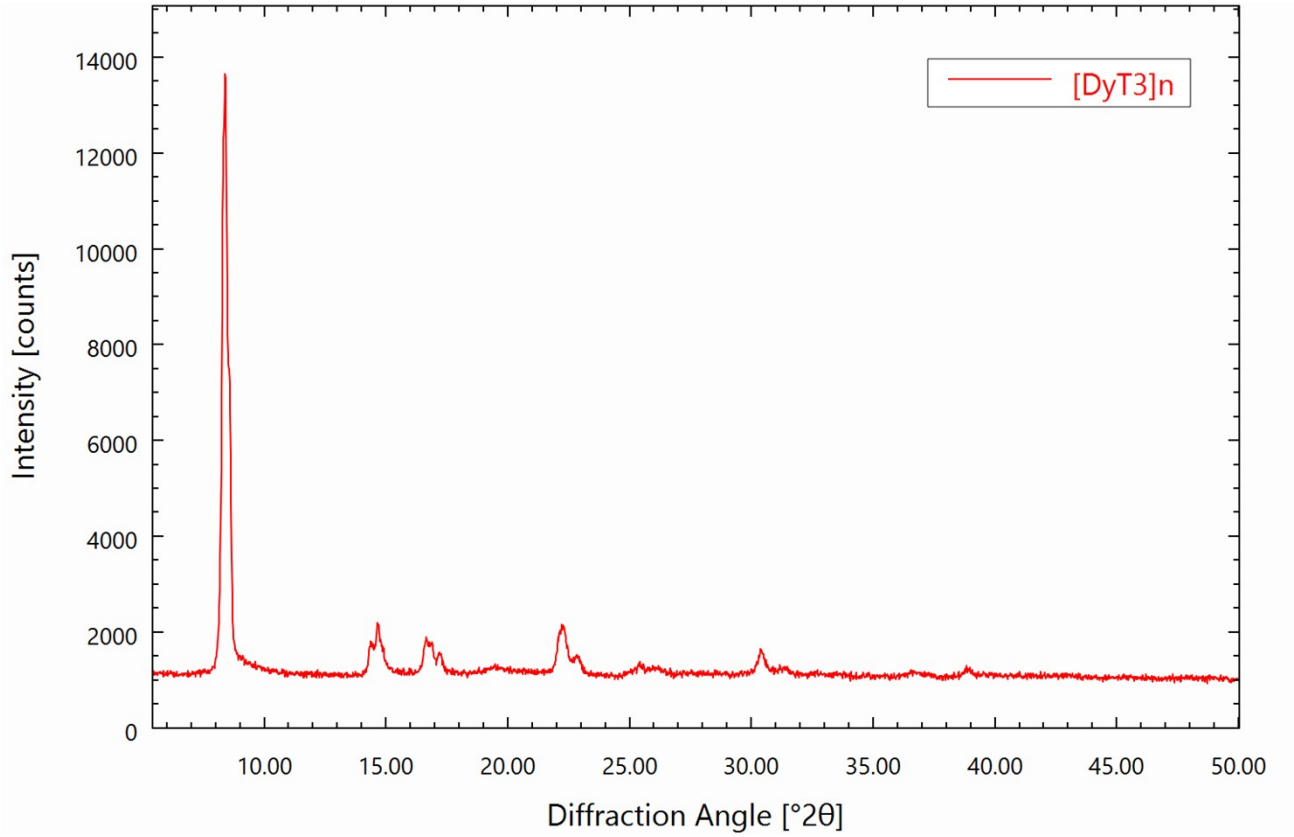

(c)

Figure S1. Powder XRD patterns (WL = 1,54060) of a **– 1Ln,** b **– 2Ln,** c – **$2Dy_n$** in comparison to the theoretical pattern for a – **$[Y(C_7H_5O_2)_3(H_2O)_2]*0.5H_2O$**, b **– $[Yb(C_7H_5O_2)_3(C_7H_6O_2)]$**.

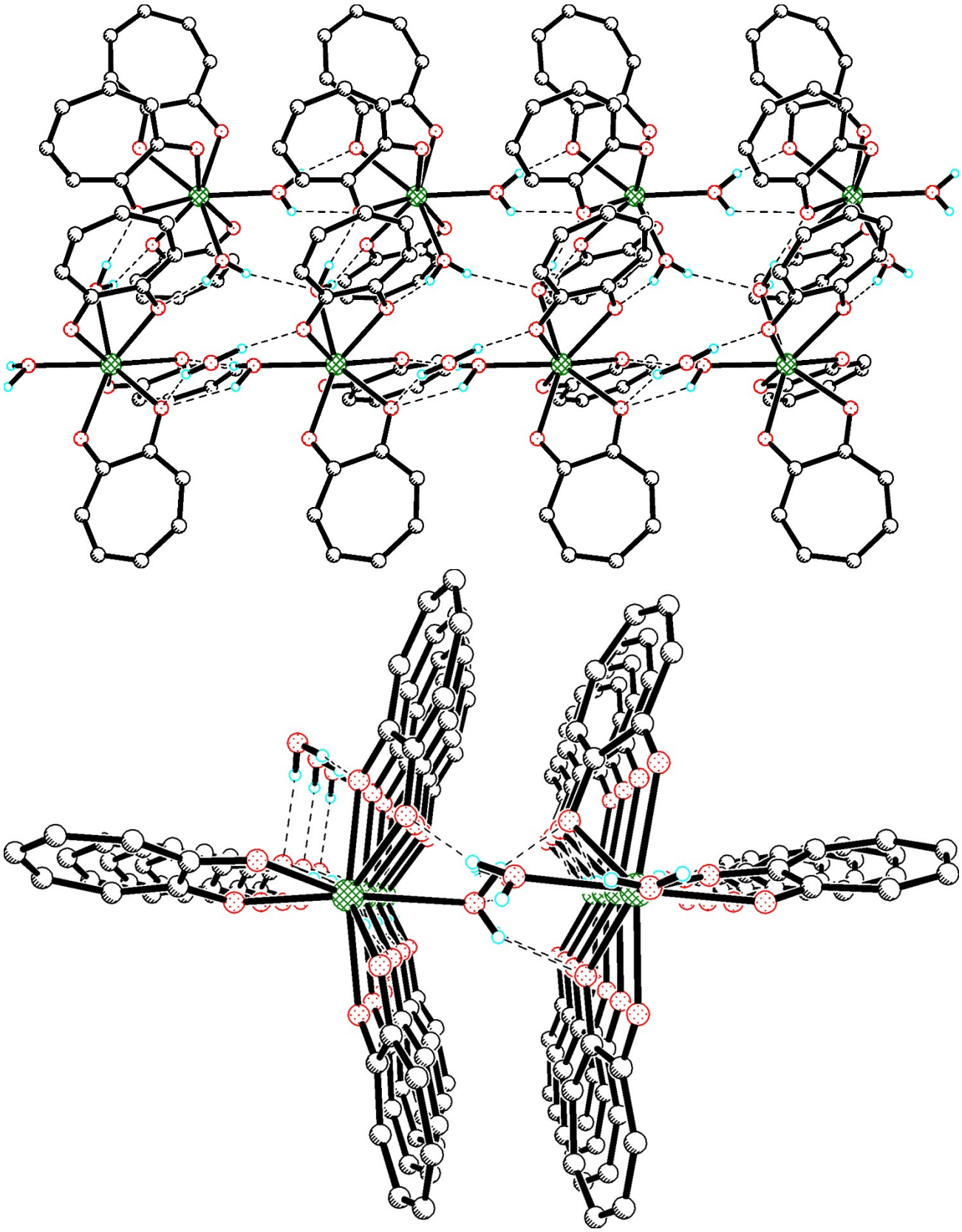

Figure S2. Two projections of a 1D chain in the structure of **1Ln**.

Table S2. SHAPE v2.1 Continuous Shape Measures calculation.

Structure*	SAPR	TDD	JBTPR	BTPR	JSD
1Er(1)	2.926	2.152	2.248	1.413	4.588
1Er(2)	2.288	1.672	2.078	1.408	3.828
2Er	2.167	1.729	2.101	1.416	3.957
2Yb_150K	2.051	1.638	2.032	1.348	3.840

* SAPR -Square antiprism; TDD -Triangular dodecahedron; JBTPR -Biaugmented trigonal prism J50; BTPR - Biaugmented trigonal prism; JSD - Snub diphenoid J84

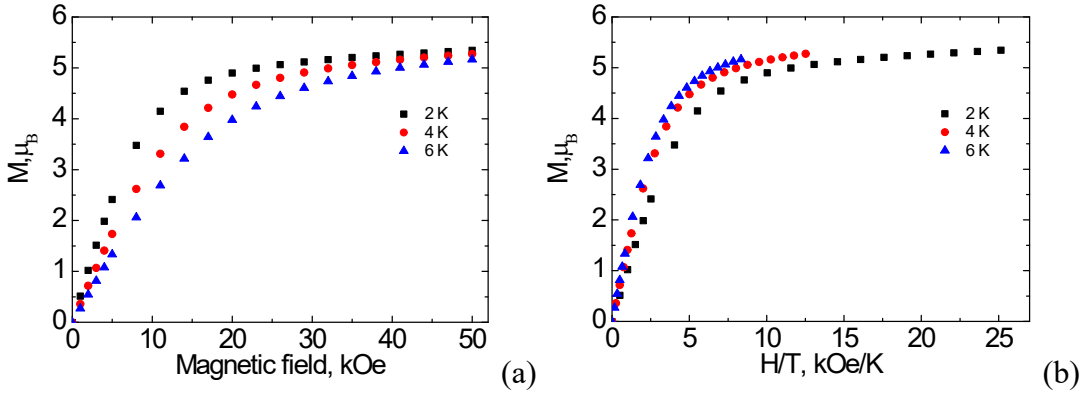

Figure S3. Dependences of the magnetization [μ_B] on the dc-magnetic field, H (a) and H/T (b) for **1Dy** at various temperatures.

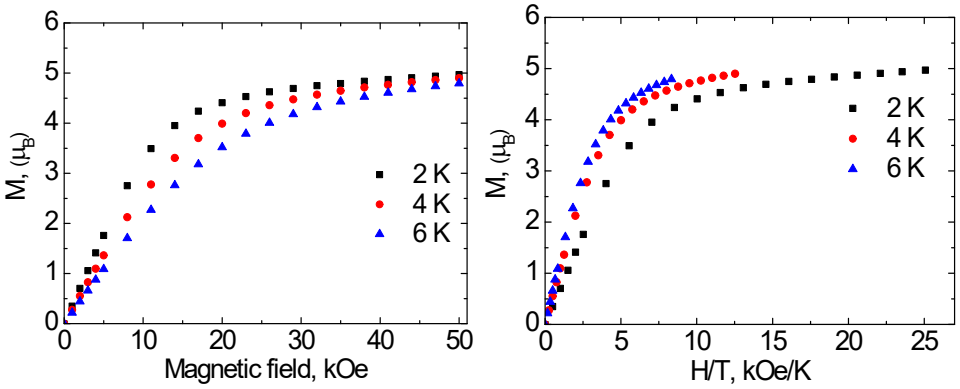

Figure S4. Dependences of the magnetization [μ_B] on the dc-magnetic field, H (a) and H/T (b) for **2Dy$_n$** at various temperatures.

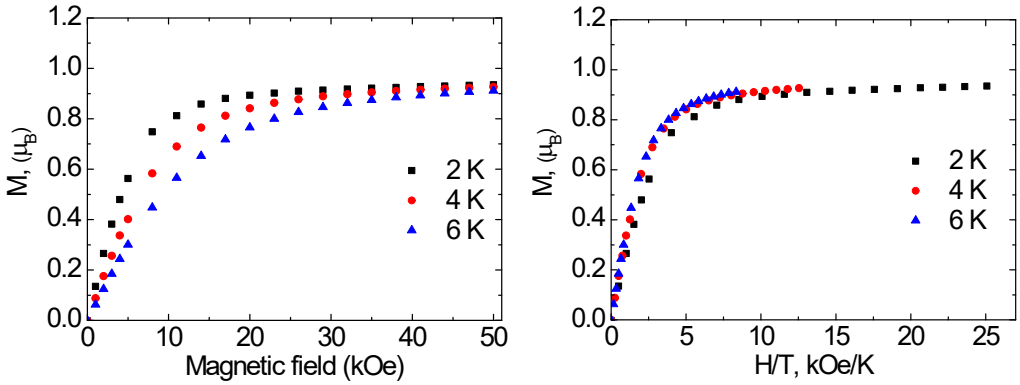

Figure S5. Dependences of the magnetization [μ_B] on the dc-magnetic field, H (a) and H/T (b) for **1DyY** at various temperatures.

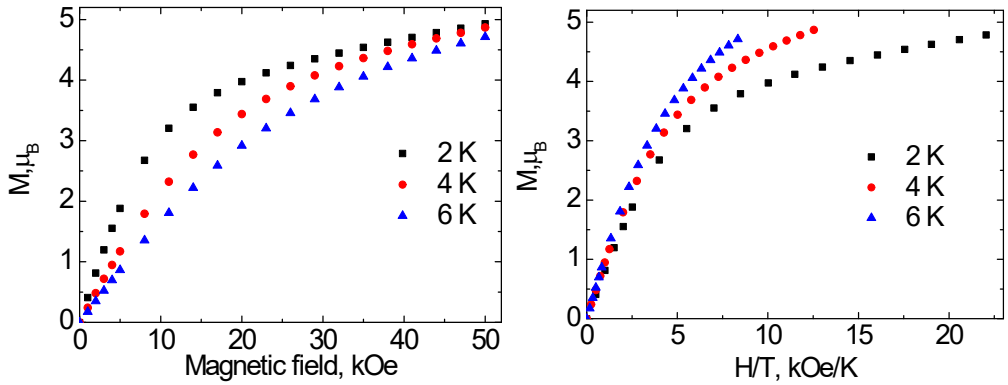

Figure S6. Dependences of the magnetization [μ_B] on the dc-magnetic field, H (a) and H/T (b) for **1Er** at various temperatures.

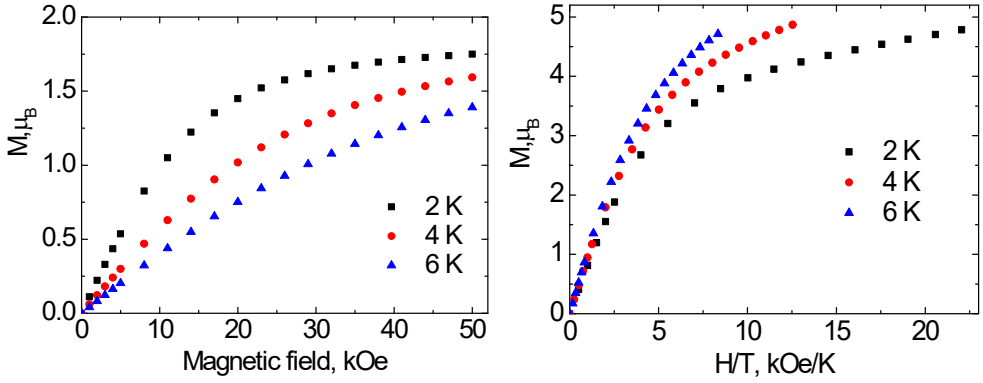

Figure S7. Dependences of the magnetization [μ_B] on the dc-magnetic field, H (a) and H/T (b) for **1Yb** at various temperatures.

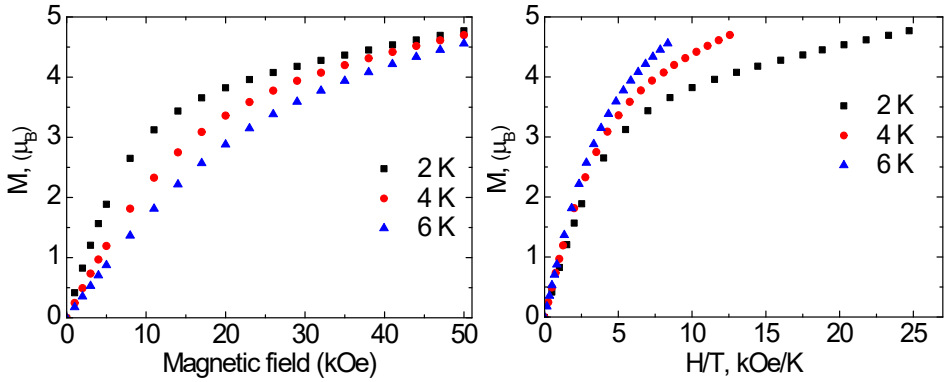

Figure S8. Dependences of the magnetization [μ_B] on the dc-magnetic field, H (a) and H/T (b) for **2Er** at various temperatures.

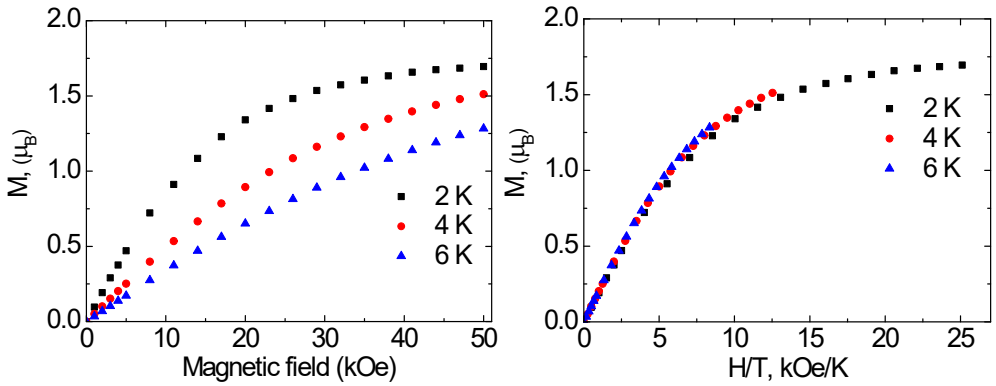

Figure S9. Dependences of the magnetization [μ_B] on the dc-magnetic field, H (a) and H/T (b) for **2Yb** at various temperatures.

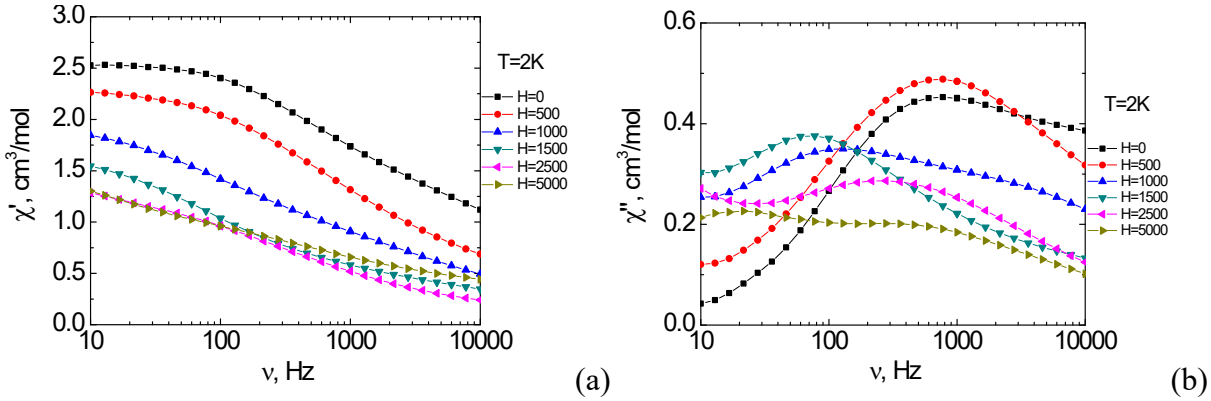

Figure S10. Frequency dependencies of the real χ' (a) and imaginary χ'' (b) components of the ac-susceptibility for complex **1Dy** in dc-magnetic fields up to 5000 Oe at 2 K.

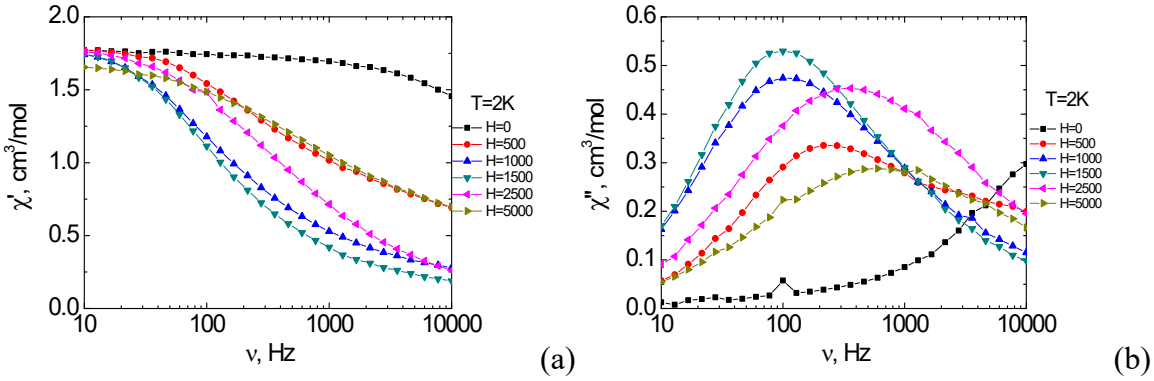

Figure S11. Frequency dependencies of the real χ' (a) and imaginary χ'' (b) components of the ac-susceptibility for complex **2Dy$_n$** in dc-magnetic fields up to 5000 Oe at 2 K.

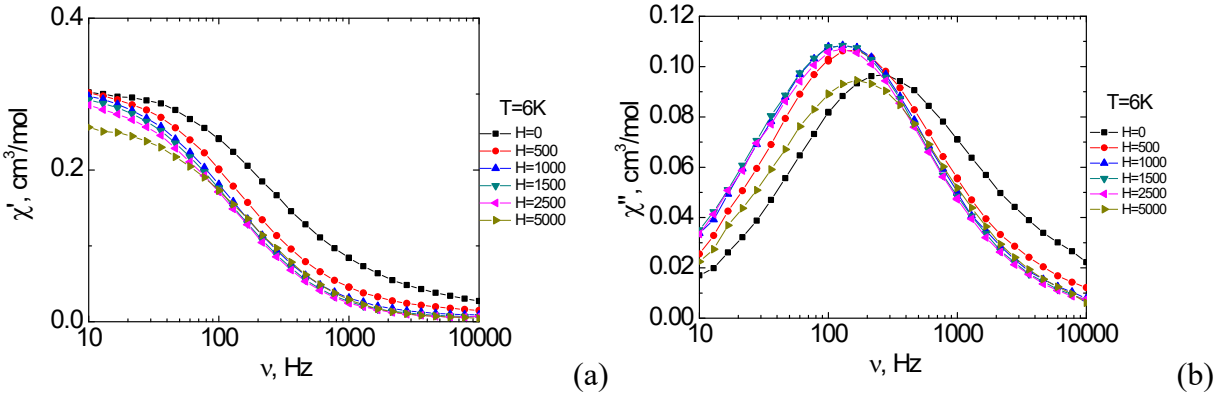

Figure S12. Frequency dependencies of the real χ' (a) and imaginary χ'' (b) components of the ac-susceptibility for complex **1DyY** in dc-magnetic fields up to 5000 Oe at 6 K.

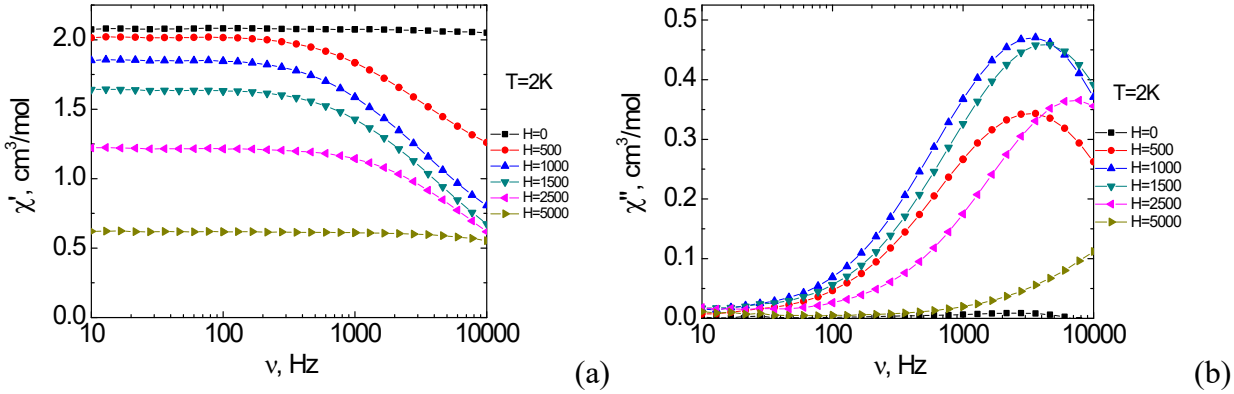

Figure S13. Frequency dependencies of the real χ' (a) and imaginary χ'' (b) components of the ac-susceptibility for complex **1Er** in dc-magnetic fields up to 5000 Oe at 2 K.

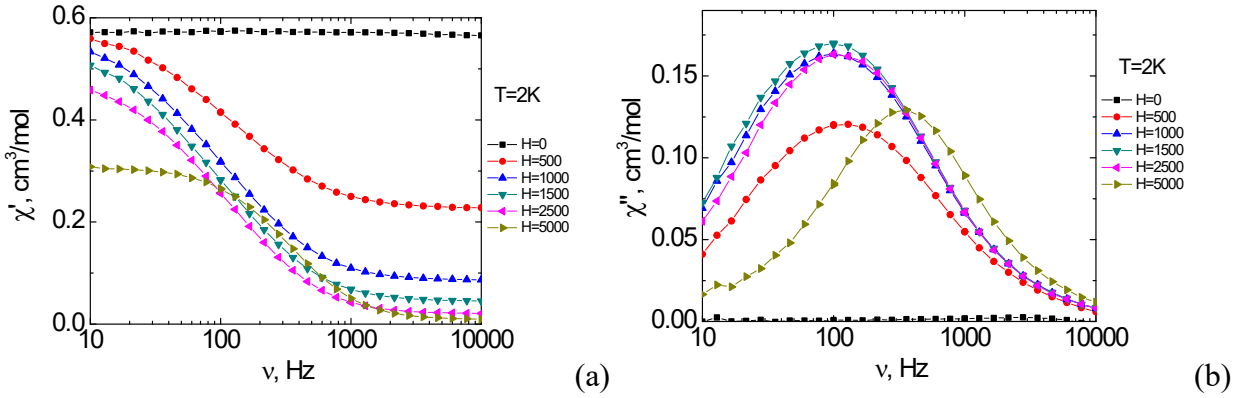

Figure S14. Frequency dependencies of the real χ' (a) and imaginary χ'' (b) components of the ac-susceptibility for complex **1Yb** in dc-magnetic fields up to 5000 Oe at 2 K.

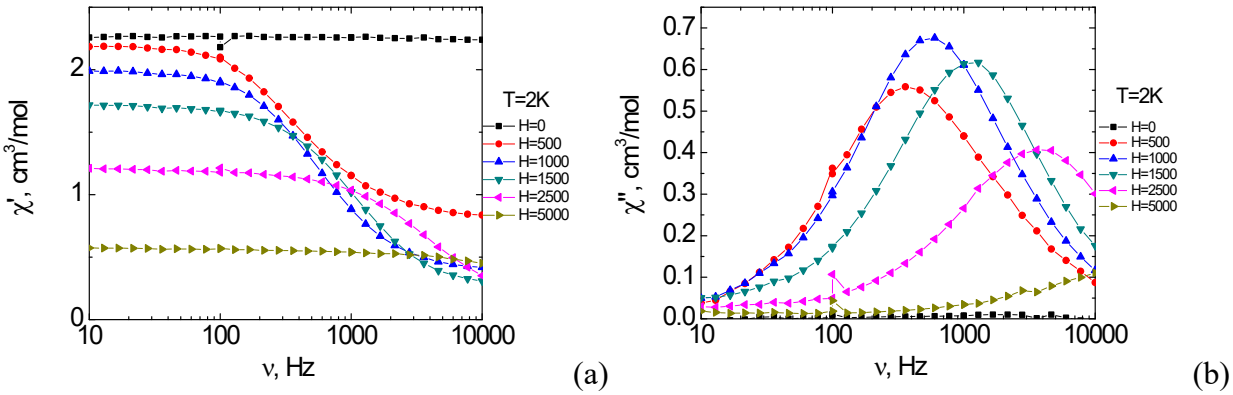

Figure S15. Frequency dependencies of the real χ' (a) and imaginary χ'' (b) components of the ac-susceptibility for complex **2Er** in dc-magnetic fields up to 5000 Oe at 2 K.

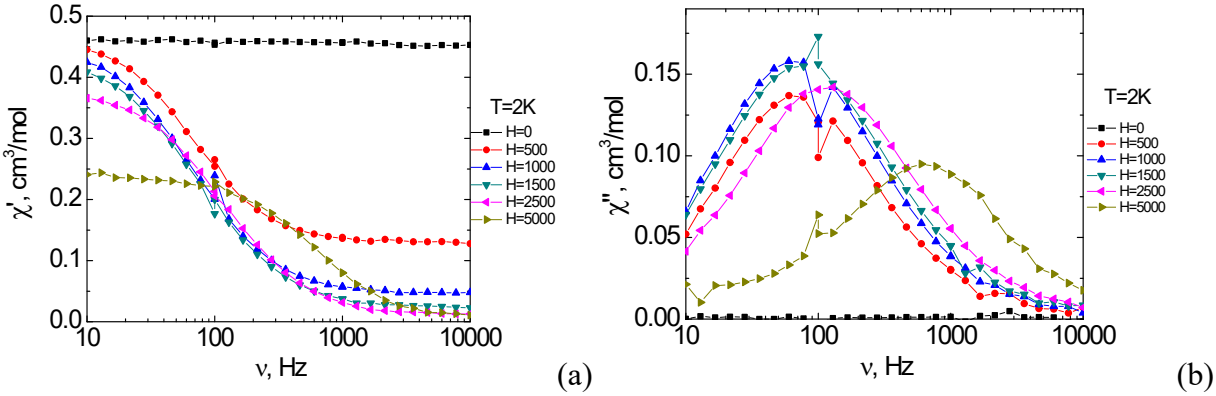

Figure S16. Frequency dependencies of the real χ' (a) and imaginary χ'' (b) components of the ac-susceptibility for complex **2Yb** in dc-magnetic fields up to 5000 Oe at 2 K.

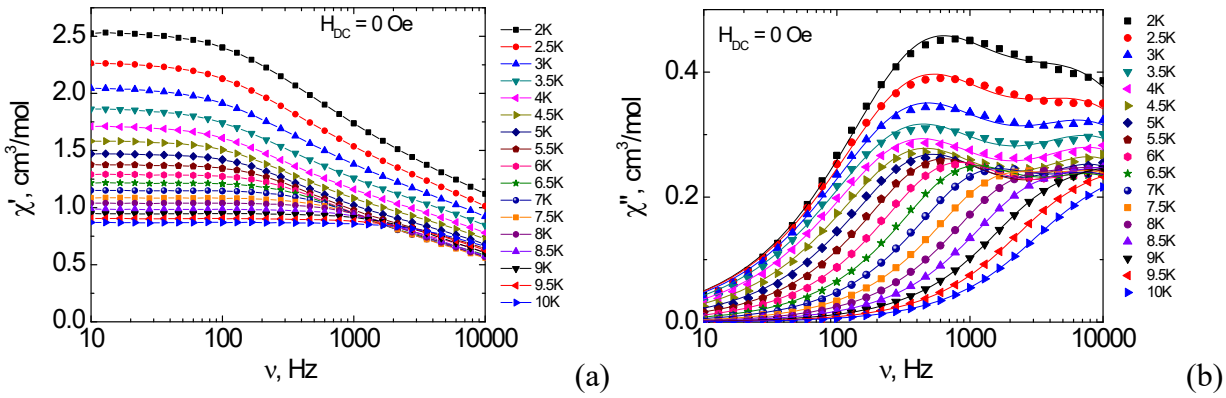

Figure S17. Frequency dependences of the real χ′(ν) (a) and imaginary χ″(ν) (b) components of dynamic magnetic susceptibility for **1Dy** (H_{dc} = 0 Oe) in the temperature range of 2-10 K. Lines on the χ′(ν) dependence are visual guides, lines on the χ″(ν) dependence are the approximations by the generalized Debye model.

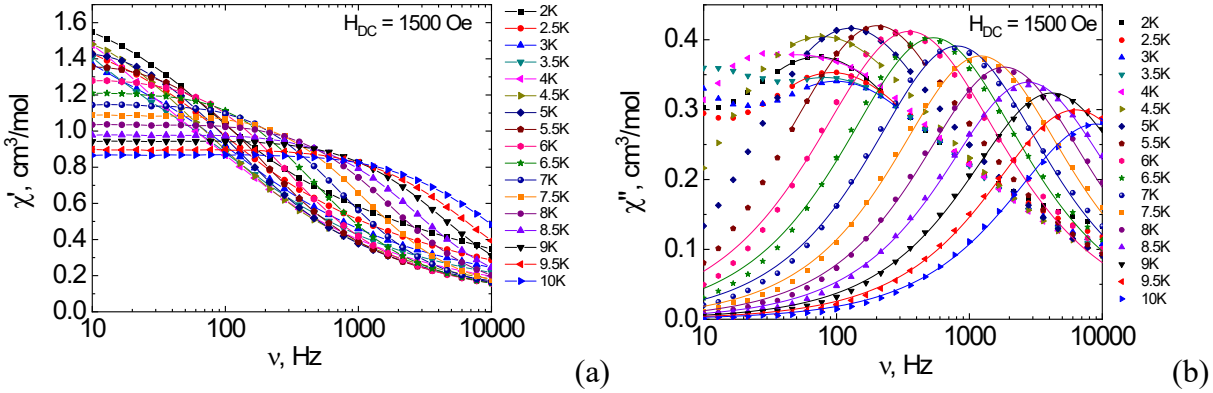

Figure S18. Frequency dependences of the real χ′(ν) (a) and imaginary χ″(ν) (b) components of dynamic magnetic susceptibility for **1Dy** (H_{dc} = 1500 Oe) in the temperature range of 2-10 K. Lines on the χ′(ν) dependence are visual guides, lines on the χ″(ν) dependence are the approximations by the generalized Debye model.

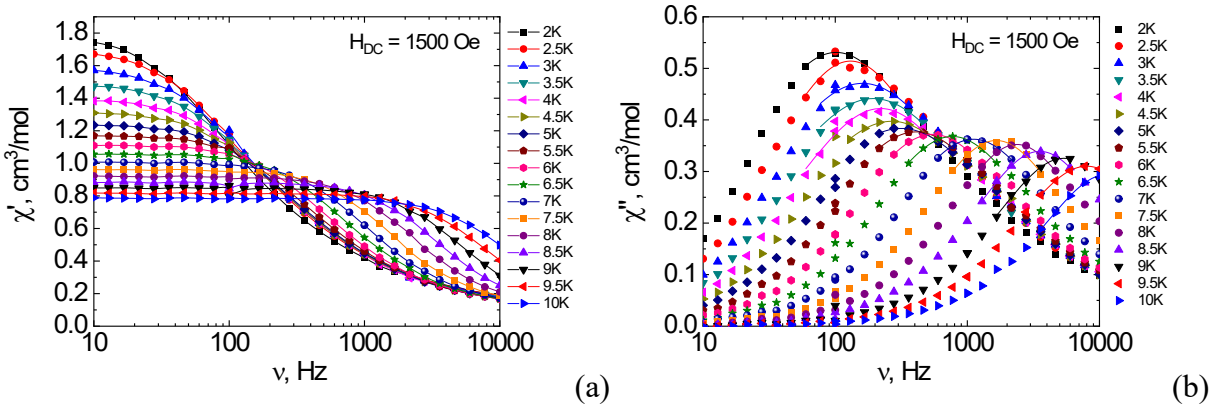

Figure S19. Frequency dependences of the real χ′(ν) (a) and imaginary χ″(ν) (b) components of dynamic magnetic susceptibility for **2Dy$_n$** (H_{dc} = 1500 Oe) in the temperature range of 2-10 K. Lines on the χ′(ν) dependence are visual guides, lines on the χ″(ν) dependence are the approximations by the generalized Debye model.

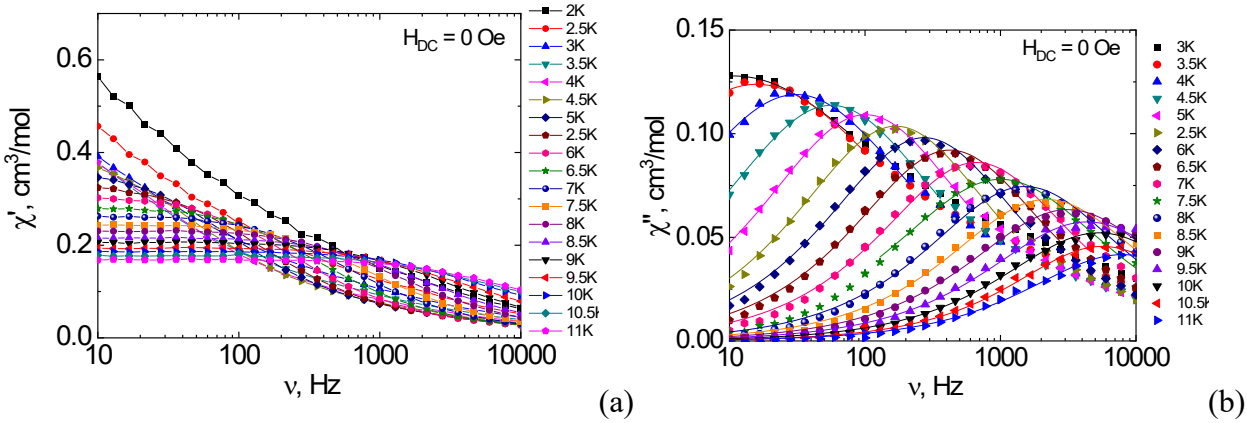

Figure S20. Frequency dependences of the real χ′(ν) (a) and imaginary χ″(ν) (b) components of dynamic magnetic susceptibility for **1DyY** (H_{dc} = 0 Oe) in the temperature range of 3-11 K. Lines on the χ′(ν) dependence are visual guides, lines on the χ″(ν) dependence are the approximations by the generalized Debye model.

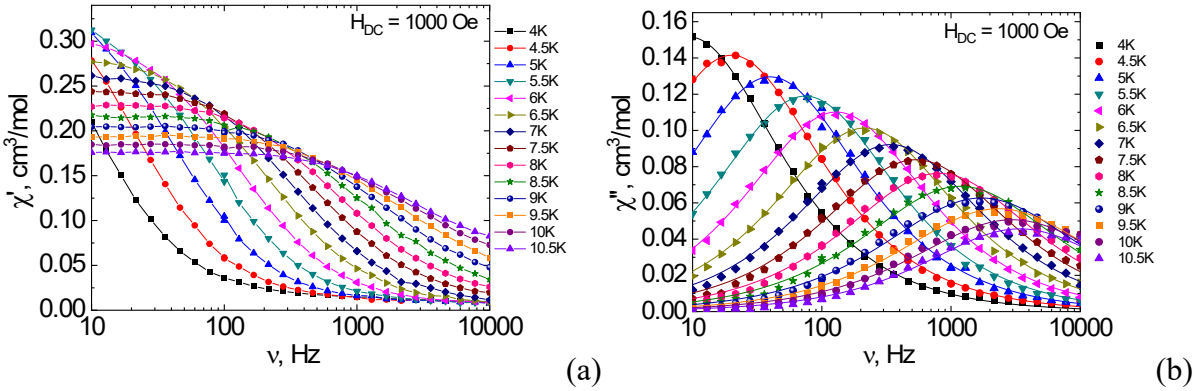

Figure S21. Frequency dependences of the real χ′(ν) (a) and imaginary χ″(ν) (b) components of dynamic magnetic susceptibility for **1DyY** (H_{dc} = 1000 Oe) in the temperature range of 4-10.5 K. Lines on the χ′(ν) dependence are visual guides, lines on the χ″(ν) dependence are the approximations by the generalized Debye model.

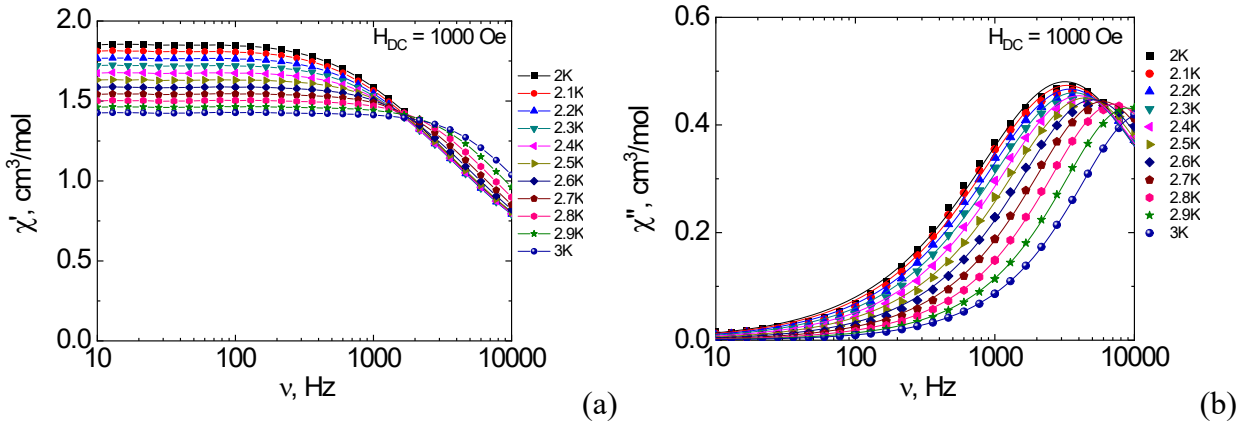

Figure S22. Frequency dependences of the real χ′(ν) (a) and imaginary χ″(ν) (b) components of dynamic magnetic susceptibility for **1Er** (H_{dc} = 1000 Oe) in the temperature range of 2-3 K. Lines on the χ′(ν) dependence are visual guides, lines on the χ″(ν) dependence are the approximations by the generalized Debye model.

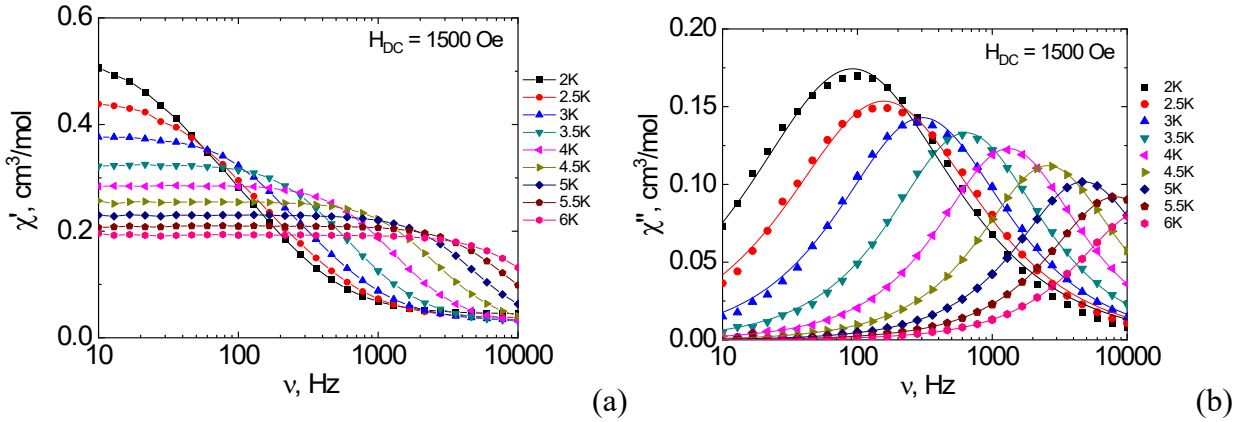

Figure S23. Frequency dependences of the real χ′(ν) (a) and imaginary χ″(ν) (b) components of dynamic magnetic susceptibility for **1Yb** (H_{dc} = 1500 Oe) in the temperature range of 2-6 K. Lines on the χ′(ν) dependence are visual guides, lines on the χ″(ν) dependence are the approximations by the generalized Debye model.

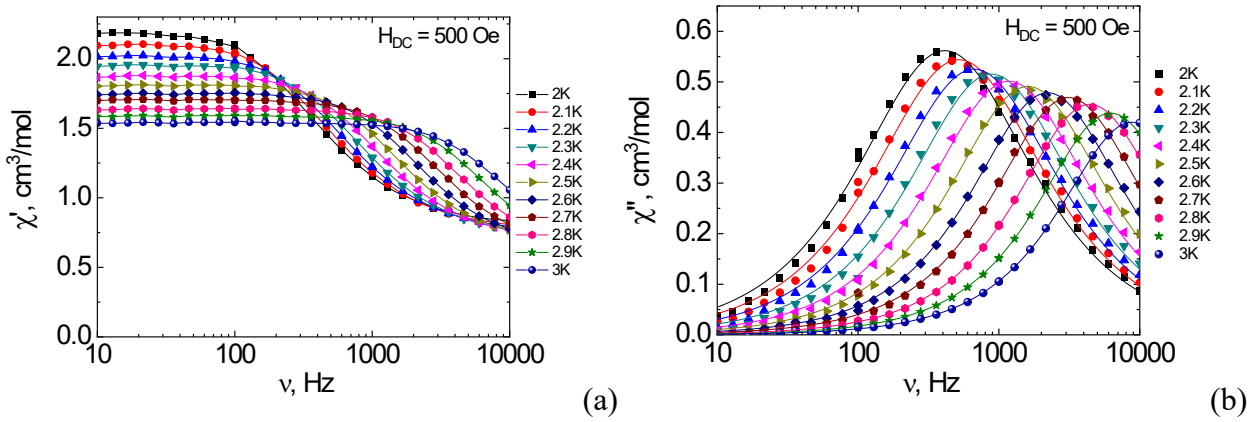

Figure S24. Frequency dependences of the real χ′(ν) (a) and imaginary χ″(ν) (b) components of dynamic magnetic susceptibility for **2Er** (H_{dc} = 500 Oe) in the temperature range of 2-3 K. Lines on the χ′(ν) dependence are visual guides, lines on the χ″(ν) dependence are the approximations by the generalized Debye model.

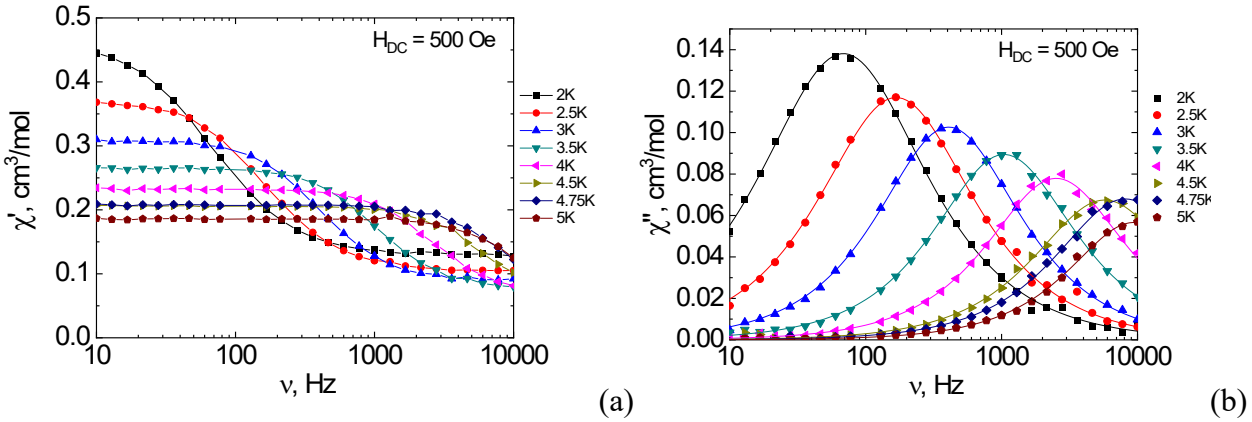

Figure S25. Frequency dependences of the real χ′(ν) (a) and imaginary χ″(ν) (b) components of dynamic magnetic susceptibility for **2Yb** (H_{dc} = 500 Oe) in the temperature range of 2-5 K. Lines on the χ′(ν) dependence are visual guides, lines on the χ″(ν) dependence are the approximations by the generalized Debye model.

Table S3. Fitting of the τ *vs.* T dependences for **1Er**.

Dependence of the relaxation time τ on the reciprocal temperature for complex **1Er** (H = 1 kOe, T = 2–2.9 K).	Fit function, temperature range, and the best-fit parameters with uncertainties.
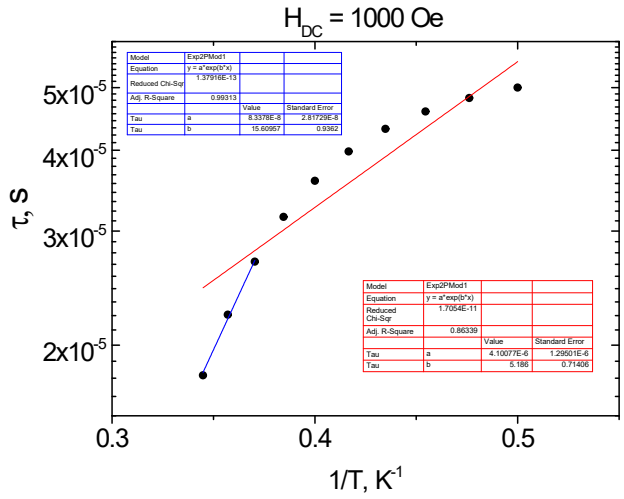	**Orbach** $\tau = \tau_0 \cdot \exp(\Delta E/kT)$ T = 2.7–2.9 K $\Delta E/k$ = 15.6±0.9 K $\tau_0 = 8 \cdot 10^{-8} \pm 3 \cdot 10^{-8}$ s R^2 = 0.99313 (blue line) T = 2-2.9 K $\Delta E/k$ = 5.2±0.7 K $\tau_0 = 4 \cdot 10^{-6} \pm 1 \cdot 10^{-6}$ s R^2 = 0.86339 (red line)

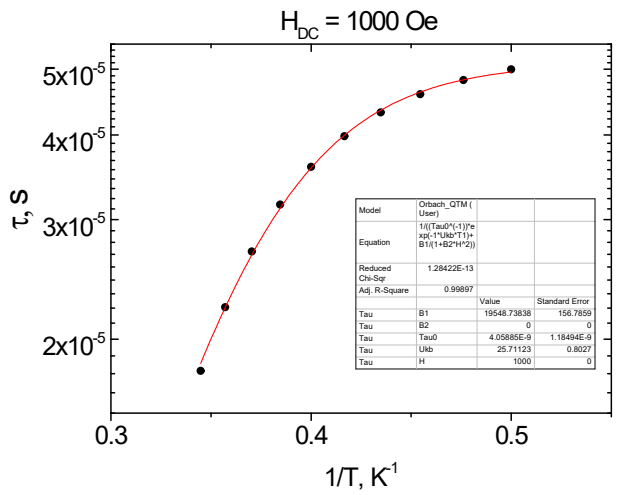

Orbach+ QTM

$\tau^{-1} = \tau_0^{-1} \cdot \exp(-\Delta E/kT) + B$

T = 2-2.9 K

$\Delta E/k$ = 25.7±0.8 K

$\tau_0 = 4 \cdot 10^{-9} \pm 1 \cdot 10^{-9}$ s

B= 19549± 157 s^{-1}

R^2 = 0.99897

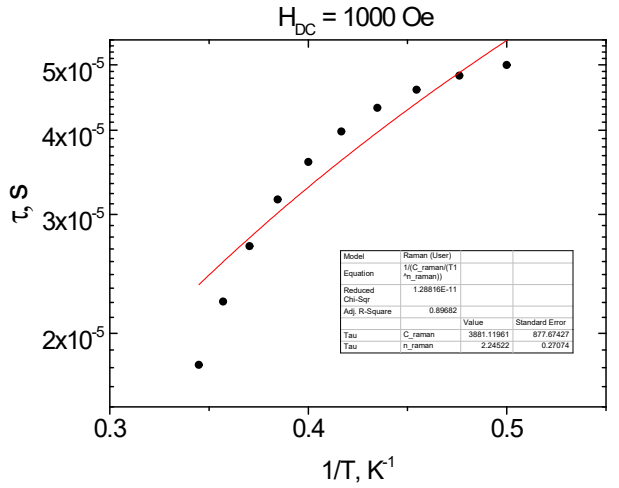

Raman

$\tau^{-1} = C_{Raman} T^{n\_Raman}$

T = 2-2.9 K

C_{Raman}= 3881±878 $s^{-1}K^{-nRaman}$

n_{Raman}= 2.2±0.3

R^2 = 0.89682

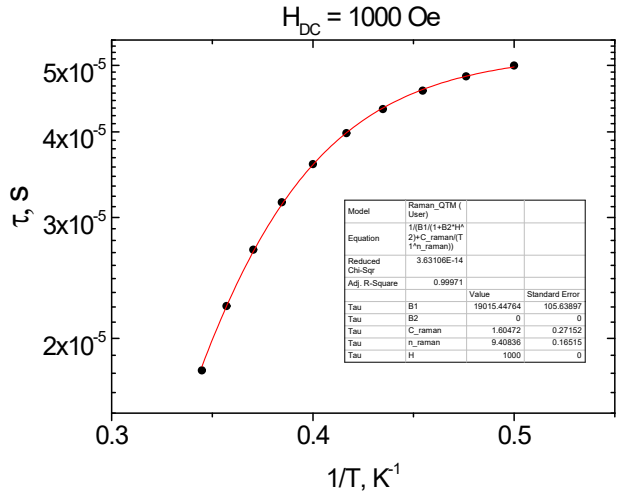

Raman+ QTM

$\tau^{-1} = C_{Raman} T^{nRaman} + B$

T = 2-2.9 K

C_{Raman}= 1.6±0.3 $s^{-1}K^{-nRaman}$

n_{Raman}= 9.4±0.2

B = 19015±106 s^{-1}

R^2 = 0.99971

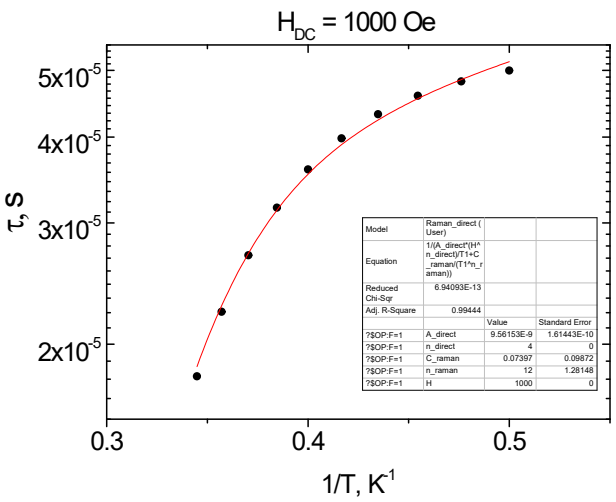

Raman+Direct

$\tau^{-1} = C_{\text{Raman}}T^{\text{nRaman}} + A_{direct}TH^4$

T = 2-2.9 K

C_{Raman}= 0.07±0.1 $s^{-1}K^{-\text{nRaman}}$

n_{Raman}= 12±1

A_{direct} = $9.6\cdot10^{-9}\pm2\cdot10^{-10}$ $K^{-1}Oe^{-4}s^{-1}$

R^2 = 0.99444

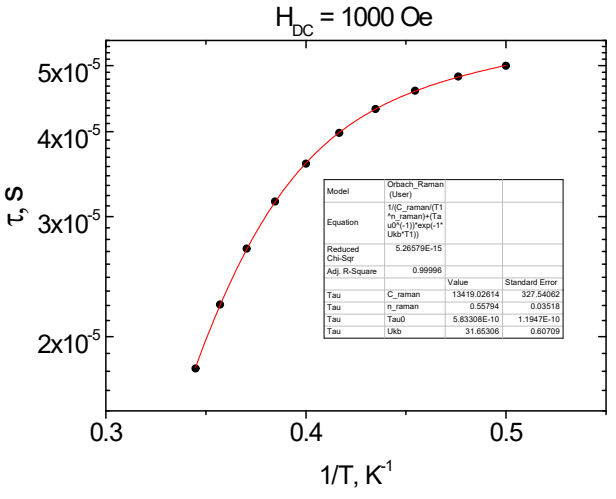

Orbach+Raman

$\tau^{-1} = \tau_0^{-1}\cdot\exp(-\Delta E/kT) + C_{\text{Raman}}T^{\text{nRaman}}$

T = 2-2.9 K

$\Delta E/k$ = 31.7±0.6 K

τ_0 = $6\cdot10^{-10}\pm1\cdot10^{-10}$ s

C_{Raman}= 13419±328 $s^{-1}K^{-\text{nRaman}}$

n_{Raman}= 0.56±0.04

R^2 = 0.99996

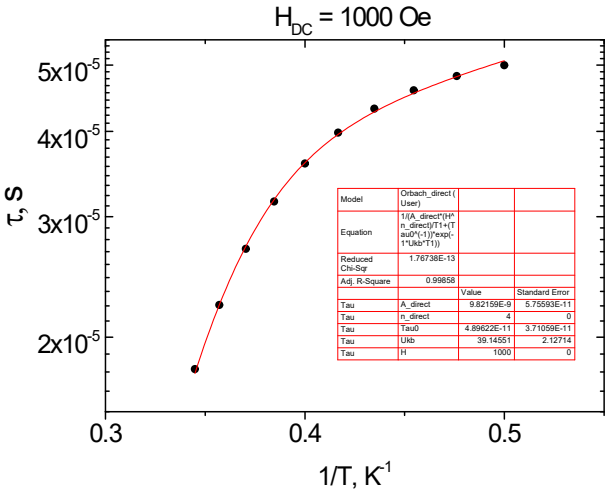

Orbach+Direct

$\tau^{-1} = \tau_0^{-1}\cdot\exp(-\Delta E/kT) + A_{direct}TH^4$

T = 2-2.9 K

$\Delta E/k$ = 39±2 K

τ_0 = $5\cdot10^{-11}\pm4\cdot10^{-11}$ s

A_{direct} = $9.82\cdot10^{-9}\pm6\cdot10^{-11}$ $K^{-1}Oe^{-4}s^{-1}$

R^2 = 0.99858

Table S4. Fitting of the τ *vs.* T dependences for **2Er**.

Dependence of the relaxation time τ on the reciprocal temperature for complex **2Er** (H = 0.5 kOe, T = 2–3 K).	Fit function, temperature range, and the best-fit parameters with uncertainties.
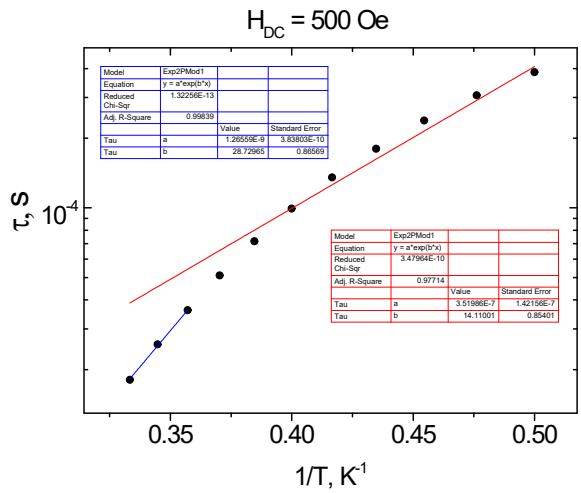	**Orbach** $\tau = \tau_0 \cdot \exp(\Delta E/kT)$ T = 2.8–3 K $\Delta E/k$ = 28.7±0.9 K $\tau_0 = 1.3 \cdot 10^{-9} \pm 4 \cdot 10^{-10}$ s R^2 = 0.99839 (blue line) T = 2-3 K $\Delta E/k$ = 14.1±0.9 K $\tau_0 = 4 \cdot 10^{-7} \pm 1 \cdot 10^{-7}$ s R^2 = 0.97714 (red line)
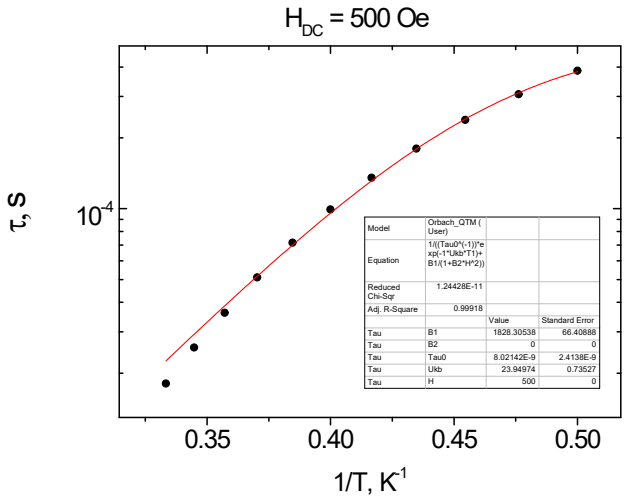	**Orbach+ QTM** $\tau^{-1} = \tau_0^{-1} \cdot \exp(-\Delta E/kT) + B$ T = 2-3 K $\Delta E/k$ = 23.9±0.7 K $\tau_0 = 8 \cdot 10^{-9} \pm 2 \cdot 10^{-9}$ s B= 1828± 66 s^{-1} R^2 = 0.99918

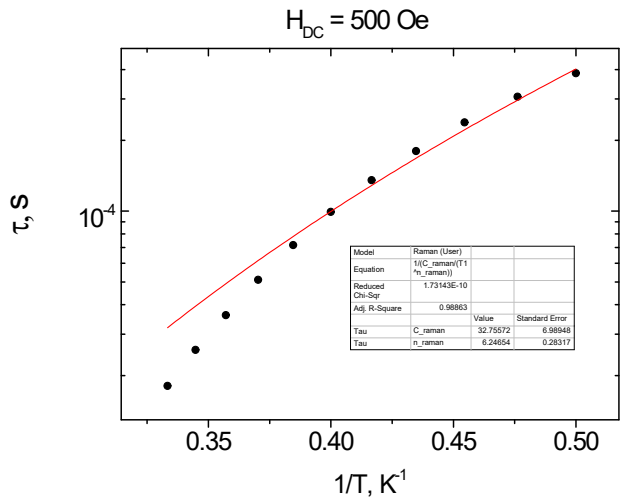

Raman

$\tau^{-1} = C_{\text{Raman}} T^{\text{n\_Raman}}$

T = 2-3 K

C_{Raman}= 33±7 $s^{-1}K^{-\text{nRaman}}$

n_{Raman}= 6.2±0.3

R^2 = 0.98863

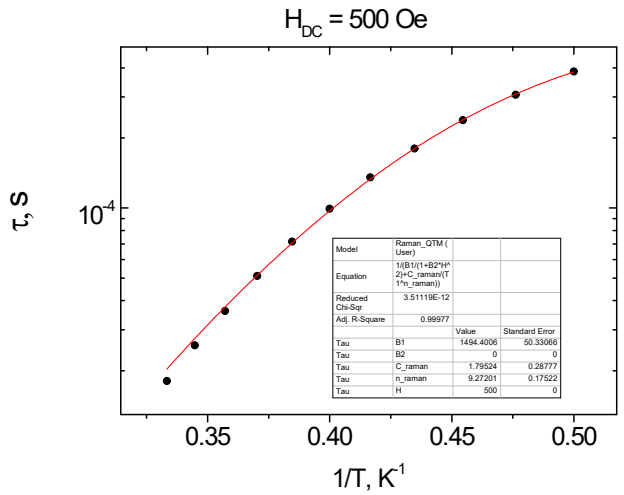

Raman+QTM

$\tau^{-1} = C_{\text{Raman}} T^{\text{nRaman}} + \text{B}$

T = 2-3 K

C_{Raman}= 1.8±0.3 $s^{-1}K^{-\text{nRaman}}$

n_{Raman}= 9.3±0.2

B = 1494±50 s^{-1}

R^2 = 0.99977

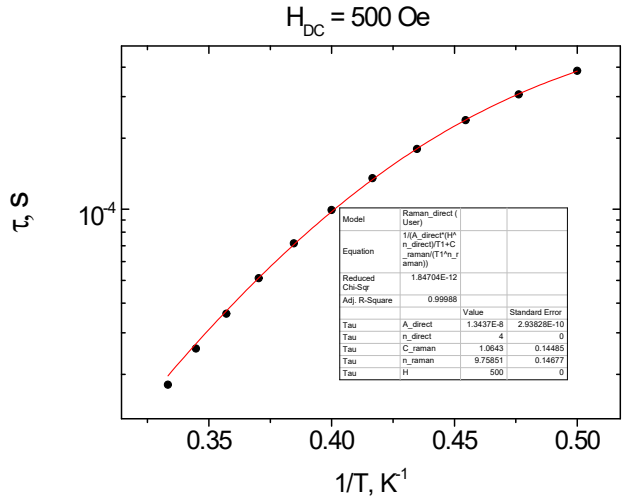

Raman+Direct

$\tau^{-1} = C_{\text{Raman}} T^{\text{nRaman}} + A_{direct} T H^4$

T = 2-3 K

C_{Raman}= 1.0±0.1 $s^{-1}K^{-\text{nRaman}}$

n_{Raman}= 9.8±0.1

A_{direct} = $1.34 \cdot 10^{-8} \pm 3 \cdot 10^{-10}$ $K^{-1}Oe^{-4}s^{-1}$

R^2 = 0.99988

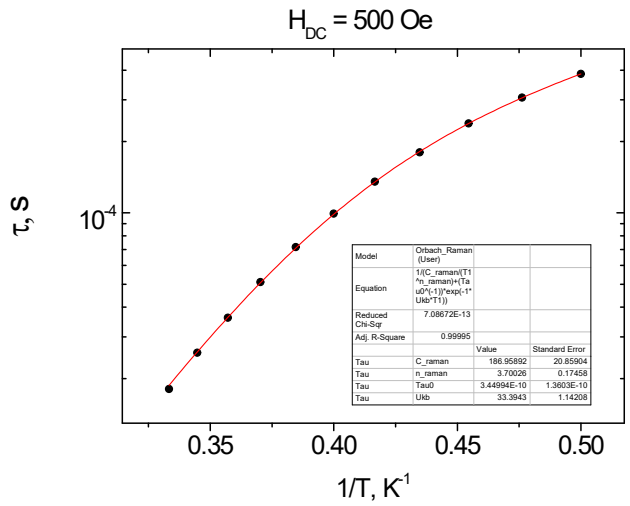

Orbach+Raman

$\tau^{-1} = \tau_0^{-1} \cdot \exp(-\Delta E/kT) + C_{\text{Raman}} T^{n\text{Raman}}$

T = 2-3 K

$\Delta E/k$ = 33±1 K

$\tau_0 = 3 \cdot 10^{-10} \pm 1 \cdot 10^{-10}$ s

$C_{\text{Raman}} = 187 \pm 21$ s^{-1}K$^{-n\text{Raman}}$

$n_{\text{Raman}} = 3.7 \pm 0.2$

$R^2 = 0.99995$

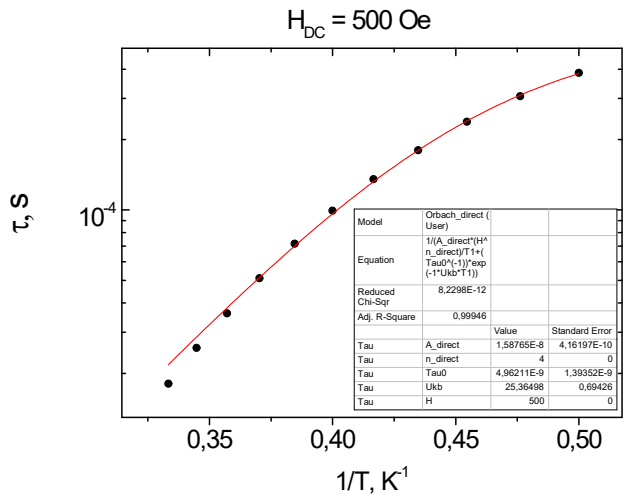

Orbach+Direct

$\tau^{-1} = \tau_0^{-1} \cdot \exp(-\Delta E/kT) + A_{direct} T H^4$

T = 2-3 K

$\Delta E/k$ = 25.4±0.7 K

$\tau_0 = 5 \cdot 10^{-9} \pm 1 \cdot 10^{-9}$ s

$A_{direct} = 1.59 \cdot 10^{-8} \pm 4 \cdot 10^{-10}$ K^{-1}Oe^{-4}s^{-1}

$R^2 = 0.99946$

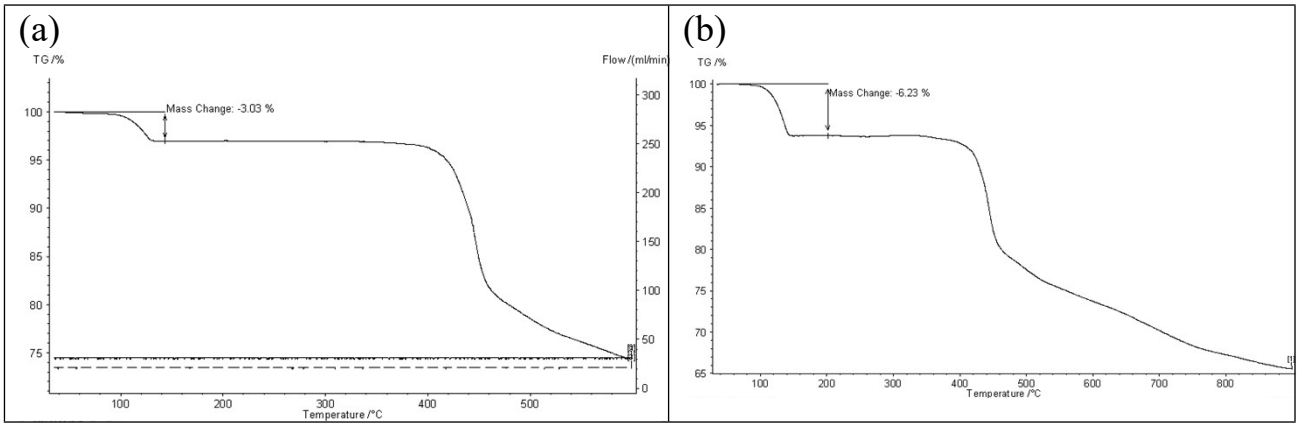

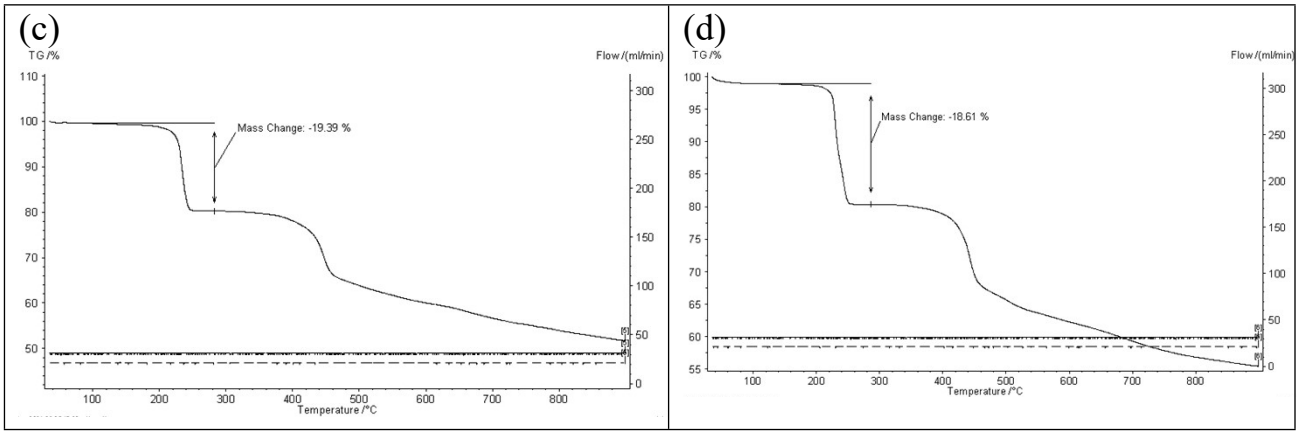

Figure S26. TG curves for **1Dy** (a), **1Er** (b), **2Er** (c), **2Yb** (d) with the mass change on the first stage of the decomposition.